Journal of Power Sources 187 (2009) 535–543

Contents lists available at ScienceDirect

Journal of Power Sources

journal homepage: www.elsevier.com/locate/jpowsour

Numerical study on micro-reformer performance and local transport phenomena of the plate methanol steam micro-reformer

Ching-Yi Hsueh[a], Hsin-Sen Chu[a], Wei-Mon Yan[b,*]

[a] Department of Mechanical Engineering, National Chiao Tung University, Hsin-Chu 300, Taiwan, ROC
[b] Department of Mechatronic Engineering, Huafan University, Shih-Ting, Taipei 223, Taiwan, ROC

ARTICLE INFO

Article history:
Received 19 September 2008
Received in revised form 3 November 2008
Accepted 5 November 2008
Available online 13 November 2008

Keywords:
Micro-reformer
Micro channel
Aspect ratio
Chemical reaction
Heat and mass transfer

ABSTRACT

The objective of this work is to investigate the transport phenomena and performance of a plate steam methanol micro-reformer. Micro channels of various height and width ratios are numerically analyzed to understand their effects on the reactant gas transport characteristics and micro-reformer performance. In addition, influences of Reynolds number and geometric size of micro channel on methanol conversion of micro-reformer and gas transport phenomena are also explored. The predicted results demonstrated that better performance is noted for a micro channel reformer with lower aspect-ratio micro channel. This is due to the larger the chemical reaction surface area for a lower aspect-ratio channel reformer. It is also found that the methanol conversion decreases with increasing Reynolds number Re. The results also indicate that the smaller micro channel size experiences a better methanol conversion. This is due to the fact that a smaller micro channel has a much more uniform temperature distribution, which in turn, fuel utilization efficiency is improved for a smaller micro channel reformer.

1. Introduction

Micro fuel cells are widely regarded as the most promising energy storage devices for mobiles, laptops, and personal digital assistants (PDA) in the 21st century due to their properties of high energy density, low noise, and low pollution. Kundu et al. [1] presented that the direct methanol fuel cell (DMFC) has still issues due to a low rate of oxidation and a high crossover rate. Therefore, methanol steam micro-reformers are being developed for use with small proton exchange membrane fuel cells (PEMFCs) to overcome these problems, and could soon become the new choice for portable fuel cell applications.

Holladay et al. [2] showed that steam reforming produces higher yields of hydrogen than autothermal reforming and partial oxidation of hydrocarbon fuels, and Kolb et al. [3] demonstrated that the plate reactors have better performance than cylindrical reactors due to better heat and mass transfer. Therefore, more studies on plate methanol steam micro-reformers are currently in progress. As a result of the steam reforming being an endothermic reaction, several researchers have used electrical heat sources to supply heat flux to steam micro-reformers [4–6]. Ha et al. [4] fabricated a PDMS (poly dimethylsiloxane) micro-reformer, and used a heater to supply heat flux. Their experimental results showed that methanol conversion was about 30–40% in the operating temperatures of 180–240 °C. The methanol conversion and hydrogen production of a plate-type micro-reformer with micro channels patterned on the micro-reformer was examined experimentally by Lim et al. [5]. The results showed approximately 78% conversion of methanol, with a hydrogen production rate of 3 L/h. Kwon et al. [6] used silicon to fabricate a reformer and preferential oxidizer (PrOx) reactor. The reformer produced hydrogen to supply the fuel cell. The measured data disclosed that the reformer generated 27 cm^3/min of hydrogen and that the CO was totally removed from the gas by the PrOx device. When the fuel cell was operating at 0.6 V, the power density was 230 mW/cm^2.

More recently, several studies have used catalytic burners to supply thermal energy to the entire micro-reformer [7–9]. Kwon et al. [7] utilized silicon fabrication technology to set up the reformer and the catalytic burner. Their results indicated that the methanol combustion reaction with the catalytic burner successfully generated heat to maintain reformer temperature. The methanol steam reformer combined with the catalytic burner produced 73% hydrogen with 65% conversion of the methanol. A micro channel methanol steam reformer which included a vaporizer, heat exchanger, catalytic combustor and steam reformer to produce hydrogen for a PEMFC was conducted experimentally by Park et al. [8]. Their results showed that at a temperature of 250 °C, the reformer could produce a gas flow rate of 450 ml/min, with a gas composition of 73.3% H_2 at the micro channel outlet. Yoshida et al. [9] fabricated a micro channel methanol reformer integrated with a

* Corresponding author. Tel.: +886 2 2663 2102; fax: +886 2 2663 1119.
E-mail address: wmyan@cc.hfu.edu.tw (W.-M. Yan).

0378-7753/$ – see front matter © 2008 Elsevier B.V. All rights reserved.
doi:10.1016/j.jpowsour.2008.11.011

Nomenclature

C_i	concentration of species i (mol m^{-3})
D_k	mass diffusion coefficient (m^2 s^{-1})
D_p	catalyst particle diameter (m)
E_a	activation energy (J mol^{-1})
H	micro channel height (m)
h_i	species enthalpy
I, J, K	grid points in the x, y and z directions, respectively
k_p	permeability (m^2)
k_1	pre-exponential factor for steam reforming
k_2	pre-exponential factor for the reverse water gas shift
L	micro channel length (m)
M_i	mole fraction of species i
$M_{w,i}$	molecular weight of species i (g mol^{-1})
m_i	mass fraction of species i
N_R	number of chemical species in the reaction
p	pressure (Pa)
q_{H_2}	hydrogen production rate at outlet (cm^3 min^{-1})
R	universal gas constant
T	temperature (°C)
T_w	wall temperature (°C)
W	micro channel width (m)
x, y, z	coordinates (m)
u, v, w	velocity components in the x, y and z directions, respectively, (m s^{-1})

Greek symbols

α	thermal diffusivity (m^2 s^{-1})
γ	aspect ratio (height and width ratio, H/W)
δ_1	catalyst layer height (m)
δ_2	flow channel height (m)
ε	porosity
η	methanol conversion
μ	viscosity (N s m^{-2})
ρ	density (kg m^{-3})

Subscripts

u	x-direction
v	y-direction
w	z-direction
0	inlet

combustor and a micro channel vaporizer. An appropriate depth of the micro channel vaporizer could generate high yields of hydrogen was found in their work.

There are many research works about the developed catalysts used in the reforming reaction using different kinetics of the methanol reforming reactions. Peppley et al. [10] studied the reaction network for methanol steam reforming over a $Cu/ZnO/Al_2O_3$ catalyst form BASF K3-110. The steam reforming of methanol over a $Cu/ZrO_2/CeO_3$ catalyst was investigated by Mastalir et al. [11]. The kinetic model suggested for the transformation involved the reverse water-gas shift and methanol decomposition, in addition to the steam reforming methanol reaction. Lee et al. [12] carried out a kinetic study of methanol steam reforming over a commercial catalyst $CuO/ZnO/Al_2O_3$.

In order to reduce the research cost and design duration, modeling and simulation are often being used to obtain a better understanding of the processes in a methanol reformer at present. Known from the literature survey, several numerical models have been presented, with the simplest methods using a one-dimensional model to describe the methanol reformer conversion and the heat and mass transport phenomena [13–18]. Kawamura et al. [13] proposed a micro channel model using mass and heat balances to analyze the transport phenomena in a plate reformer. They successfully simulated methanol conversion and gas concentration distributions along the micro channel. A mathematical model of a plate methanol steam reformer to investigate the transport phenomena was studied numerically by Kim and Kwon [14]. Their results showed that smaller reformer volumes required a higher heat flux. Varesano et al. [15] used a one-dimensional transient mathematical model to study the transport behaviors in a steam reforming reformer with a burner. The transient characteristics of the reformer were examined by Amphlett et al. [19] using the reforming kinetics. Pattekar and Kothare [16] developed one-dimensional models for radial and micro channel methanol reformers. Their results demonstrated that radial reformers have better hydrogen production rates and lower pressure drops than micro channel reformers. A transient model for packed-bed catalytic methanol reformers was performed by Stamps and Gatzke [17]. They found that agreement of the theoretical and experimental results for the temperature, flow rate and CO concentration data. Lattner and Harold [18] have numerically and experimentally investigated a bench-scale fixed-bed methanol reformer for autothermal reforming. This system was also used by Pepply et al. [20] and Reitz et al. [21] who presented kinetic rate expressions for the simulations. Their results showed agreement between the theoretical and experimental results.

As for the two-dimensional simulation about the methanol reformers, the literature survey has existed in the past decade. Suh et al. [22] proposed a cylindrical mathematical model of a packed bed reformer to investigate the heat and mass transfer for different species in a reformer. The results indicated that the predicted methanol conversion rates were compared well with the experimental data. A mathematical model of a cylindrical reformer to investigate the methanol conversion in a packed bed reformer and a wall-coated reformer was proposed by Karim et al. [23,24]. Their results showed that the minimum reformer diameter yielded the highest catalyst activity and smallest temperature gradient. The results also showed that wall-coated reformers have higher catalytic activity and lower pressure drops than packed-bed reformers do.

There are many three-dimensional simulations of methanol reformers in the literature. A cylindrical model of the reformer which comprised of a methanol steam reformer and a CO methanator to simulate the conversion and temperature distributions in the reformer was investigated by Cao et al. [25]. Pan and Wang [26] developed a numerical model for a plate-fin reformer which integrated endothermic and exothermic reactions into one unit. Their numerical model accurately predicted the methanol conversion and the gas distributions. Numerical simulation of transport phenomena of the plate micro-scale methanol reformer was examined by Pattekar and Kothare [27]. Park et al. [28] developed three-dimensional, quasi three-dimensional and one-dimensional models to study the plate methanol reformers. Cao et al. [29] presented kinetic rate expressions and developed a homogenous model of a micro channel reformer to simulate the temperature distributions in a micro channel.

The geometric design of a reactor is one of the most important issues. Appropriate reactor geometry can improve the reactant gas transport and the efficiency of thermal management [20,21,30–36]. To this end, Kundu et al. [37] used different flow configurations including serpentine and parallel flow fields to improve plate methanol reformer performance. As stated above, while many studies have investigated the effects of reactor radius on cylindrical reactor performance [23,24,32–36], few studies have reported on the flow channel designs of plate methanol steam micro-reformers. Therefore, based on flow channel designs, various aspect ratios of micro channels on plate methanol steam micro-reformers can

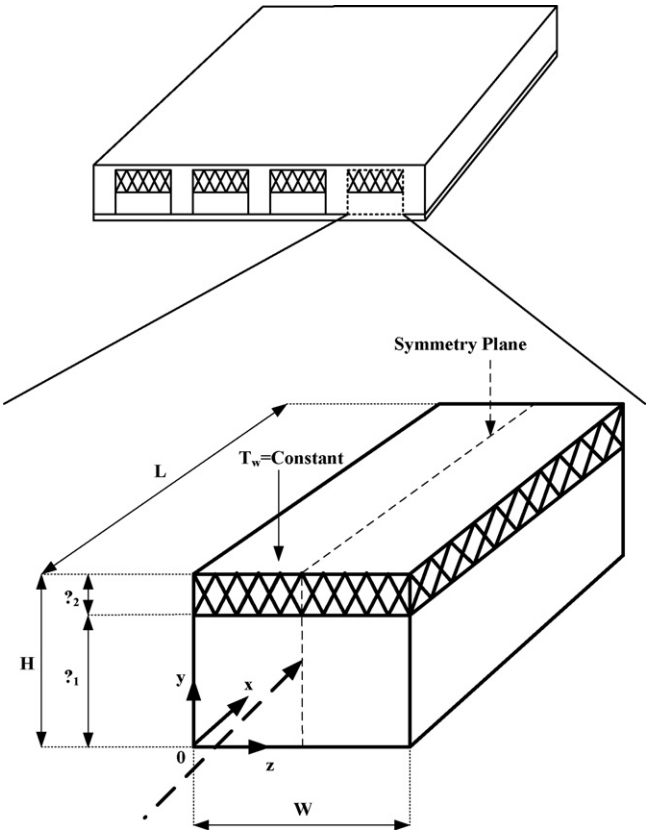

Fig. 1. Schematic diagram of the present study.

potentially enhance fuel utilization. In this work, flow channels with various aspect ratios (height and width ratios) and geometric size are numerically examined the transport phenomena in a micro channel reformer. In addition, the thermo-fluid parameters (Reynolds number and wall temperature) are also investigated to examine their effects on the methanol conversion and efficiency of micro channel reformers.

2. Analysis

In the present study, a three-dimensional micro channel model of the plate methanol steam micro-reformer was proposed to analyze the local transport phenomena and micro-reformer performance. The micro channel is comprised of the flow channel and a catalyst layer. Therefore, the governing equations include mass, momentum, energy and species equations. For simplicity, the following assumptions are made:

(1) The flow is steady state.
(2) The inlet fuel is an ideal gas.
(3) The flow is laminar and incompressible.
(4) The catalyst layer is isotropic.
(5) The chemical reaction occurs only in the catalyst layer.
(6) Thermal radiation and conduction in the gas phase are negligible compared to convection.

To reduce the computing time, the symmetric micro channel is considered only in this work. The schematic diagram of this work is shown in Fig. 1. The various cases for different aspect ratios are shown in Table 1. The aspect ratios, γ, are defined as follows:

$$\gamma = \frac{H}{W} \tag{1}$$

Table 1
The cases with various aspect-ratio micro channels used in this work.

	Case 1	Case 2	Case 3	Case 4
γ	0.25	0.5	1.0	2.0
H (mm)	0.179	0.214	0.286	0.429
W (mm)	0.714	0.429	0.286	0.214

where H and W are the micro channel height and width, respectively. The corresponding hydraulic diameters in Table 1 are fixed to be 0.286 mm.

The governing equations under the assumptions stated above can be defined as follows:

Continuity equation:

$$\varepsilon\rho\left(\frac{\partial u}{\partial x}+\frac{\partial v}{\partial y}+\frac{\partial w}{\partial z}\right)=0 \tag{2}$$

X-momentum equation:

$$\varepsilon\rho\left(u\frac{\partial u}{\partial x}+v\frac{\partial u}{\partial y}+w\frac{\partial u}{\partial z}\right)=-\varepsilon\frac{\partial p}{\partial x}+\varepsilon\mu\left(\frac{\partial^2 u}{\partial x^2}+\frac{\partial^2 u}{\partial y^2}+\frac{\partial^2 u}{\partial z^2}\right)+S_u \tag{3}$$

Y-momentum equation:

$$\varepsilon\rho\left(u\frac{\partial v}{\partial x}+v\frac{\partial v}{\partial y}+w\frac{\partial v}{\partial z}\right)=-\varepsilon\frac{\partial p}{\partial y}+\varepsilon\mu\left(\frac{\partial^2 v}{\partial x^2}+\frac{\partial^2 v}{\partial y^2}+\frac{\partial^2 v}{\partial z^2}\right)+S_v \tag{4}$$

Z-momentum equation:

$$\varepsilon\rho\left(u\frac{\partial w}{\partial x}+v\frac{\partial w}{\partial y}+w\frac{\partial w}{\partial z}\right)$$
$$=-\varepsilon\frac{\partial p}{\partial y}+\varepsilon\mu\left(\frac{\partial^2 w}{\partial x^2}+\frac{\partial^2 w}{\partial y^2}+\frac{\partial^2 w}{\partial z^2}\right)+S_w \tag{5}$$

S_u, S_v and S_w denote source terms based on the Darcy drag forces in the x, y and z directions imposed by the pore walls on the fluid which usually cause significant pressure drops across the porous media. In this work, the flow channel is not a porous medium, therefore, S_u, S_v and S_w are zero in the flow channel. However, the catalyst layer is a porous medium, so the source terms in the momentum equations for the fluid flow in the porous media are:

$$S_u=-\frac{\mu u}{k_p}-\frac{\beta u\rho}{2}\sqrt{u^2+v^2+w^2} \tag{6}$$

$$S_v=-\frac{\mu v}{k_p}-\frac{\beta v\rho}{2}\sqrt{u^2+v^2+w^2} \tag{7}$$

$$S_u=-\frac{\mu w}{k_p}-\frac{\beta w\rho}{2}\sqrt{u^2+v^2+w^2} \tag{8}$$

where k_p is the permeability and β is inertial loss coefficient in each component direction [38].

$$k_p=\frac{{D_p}^2\varepsilon^3}{150(1-\varepsilon)^2} \tag{9}$$

$$\beta=\frac{3.5(1-\varepsilon)}{D_p\varepsilon^3} \tag{10}$$

Species equation:

$$\varepsilon\left(u\frac{\partial C_i}{\partial x}+v\frac{\partial C_i}{\partial y}+w\frac{\partial C_i}{\partial z}\right)=D_{\text{eff}}\left(\frac{\partial^2 C_i}{\partial x^2}+\frac{\partial^2 C_i}{\partial y^2}\frac{\partial^2 C_i}{\partial z^2}\right)+\varepsilon S_c \tag{11}$$

In the species equation, C_i denotes the concentration of the ith species: the calculations included CH_3OH, H_2O, H_2, CO_2 and CO. In Eq. (11), the effective mass diffusivity D_{eff} is expressed as $D_{\text{eff}}=\varepsilon^\tau D_k$, where ε is the porosity of the medium and τ is the tortuosity of the porous medium. In this work, τ is set to be 1, and the porosity ε is

expressed as 0.38 and 1.00, respectively, in the catalyst layer and the flow channel. In the present study, there is no chemical reaction in the flow channel, therefore, S_c is zero in flow channel. In the catalyst layer, the source term of the concentration equation, S_c, stands for the modified concentration term produced by the chemical reaction. S_c is the sum of the Arrhenius reaction sources over the N_R reactions that the species participle in:

$$S_c = M_{w,i} \sum_{r=SR,rWSG}^{N_R} R_{i,r} \tag{12}$$

where $M_{w,i}$ is the molecular weight of species i and $R_{i,r}$ is the Arrhenius molar rate of creation and destruction of species i in the reaction r. According to the simple reaction model of Purnama et al. [39], the steam reforming reaction is much faster than the decomposition and water-gas shift reaction. Therefore, only the steam reforming reaction, Eq. (13) and the water-gas shift reaction, Eq. (14) are considered in this work.

$$CH_3OH + H_2O \xrightarrow{k_1} CO_2 + 3H_2 \tag{13}$$

$$CO + H_2O \underset{k_{-2}}{\overset{k_2}{\rightleftarrows}} CO_2 + H_2 \tag{14}$$

Using the model for steam reforming of methanol by Pan and Wang [26], who presented the following mole rate of creation/destruction of species i in the SR reaction and the rWGS reaction:

$$R_{i,SR} = k_1 C_{CH_3OH}^{0.6} C_{H_2O}^{0.4} \exp\left(-\frac{E_a}{RT}\right) \tag{15}$$

$$R_{i,rWSG} = k_2 C_{CO_2} C_{H_2} \exp\left(-\frac{E_a}{RT}\right) - k_{-2} C_{CO} C_{H_2O} \exp\left(-\frac{E_a}{RT}\right) \tag{16}$$

Where the steam reforming reaction is a non-reversible reaction and the reverse water-gas shift reaction is reversible. The constants, k_1 and k_2, are forward rate constants for the steam reforming reaction and the reverse water-gas shift reaction, respectively. The constant, k_{-2}, is the backward rate constant for the water-gas shift reaction.

Energy equation:

$$\rho c_p \left(u\frac{\partial T}{\partial x} + v\frac{\partial T}{\partial y} + w\frac{\partial T}{\partial z}\right) = k_{eff}\left(\frac{\partial^2 T}{\partial x^2} + \frac{\partial^2 T}{\partial y^2} + \frac{\partial^2 T}{\partial z^2}\right) + S_t \tag{17}$$

In the energy equation, the effective thermal conductivity in the porous medium, k_{eff}, is the volume average of the fluid conductivity and solid conductivity.

$$k_{eff} = \varepsilon k_f + (1-\varepsilon)k_s \tag{18}$$

where k_f is fluid phase thermal conductivity, k_s is the solid medium thermal conductivity and ε is the porosity of the medium.

Source term, S_t, in Eq. (17) includes the heat flux due to the chemical reactions. In this work, the catalyst layer experiences exothermic chemical reactions, therefore, S_t for the chemical reactions is:

$$S_t = -\sum_i \left(\frac{h_i^0}{M_{w,i}} + \int_{Tref,i}^{T} c_{p,i}\,dT\right)(R_{i,r}) \tag{19}$$

where h_i^0 is the enthalpy of formation of species i, and R_i is the volumetric rate of creation of species i.

The boundary conditions of the present computation include those at the inlet, outlet, wall, and the interface between the flow channel and the catalyst layer. The inlet flow velocity is constant, the inlet gas compositions are constant, and the inlet temperature is constant.

$$u = u_0 \tag{20}$$

Table 2
Parameters used in this study.

Micro channel length L (m) [40]	3.3×10^{-2}
Micro channel width W (m) [40]	5.0×10^{-4}
Micro channel height H (m) [40]	2.0×10^{-4}
Catalyst layer thickness δ_1 (m)	3.0×10^{-5}
Flow channel height δ_2 (m)	1.7×10^{-4}
Average inlet temperature (°C) [40]	120
Operating pressure (atm) [40]	1
Activation energy for steam reforming (J mol^{-1}) [26]	7.6×10^4
Activation energy for reverse water gas shift (J mol^{-1}) [26]	1.08×10^5
Catalyst density (kg m^{-3}) [23]	890
Catalyst layer porosity [27]	0.38
Catalyst permeability (m^2) [27]	2.379×10^{-12}

$$C_i = C_{0,i} \tag{21}$$

$$T = T_0 \tag{22}$$

At the micro channel outlet ($x = L$), fully developed flow is assumed and the boundary conditions of velocity, temperature and concentration can be expressed as:

$$\frac{\partial u}{\partial x} = v = w = \frac{\partial C_i}{\partial x} = \frac{\partial T}{\partial x} = 0 \tag{23}$$

At the interface between the flow channel and the insulated plates ($y = 0$), the velocities and the temperature and concentration gradients are zero.

$$u = v = w = \frac{\partial C_i}{\partial y} = \frac{\partial T}{\partial y} = 0 \tag{24}$$

At the interface between the flow channel and the catalyst layer ($y = H_1 - \delta_2$), the velocities, temperature, species concentration, and species flux are continuous.

$$u_{y=(H_1-\delta_2)^+} = u_{y=(H_1-\delta_2)^-},\quad \varepsilon \left.\frac{\partial u}{\partial y}\right|_{y=(H-\delta_2)^+} = \left.\frac{\partial u}{\partial y}\right|_{y=(H-\delta_2)^-} \tag{25}$$

$$w_{y=(H_1-\delta_2)^+} = w_{y=(H_1-\delta_2)^-},\quad \varepsilon \left.\frac{\partial w}{\partial y}\right|_{y=(H-\delta_2)^+} = \left.\frac{\partial w}{\partial y}\right|_{y=(H-\delta_2)^-} \tag{26}$$

$$C_{i,y=(H_1-\delta_2)^+} = C_{i,y=(H_1-\delta_2)^-},\ D_{eff,(H-\delta_2)^+}\left.\frac{\partial C_i}{\partial y}\right|_{y=(H-\delta_2)^+} = D_{eff,(H-\delta_2)^-}\left.\frac{\partial C_i}{\partial y}\right|_{y=(H-\delta_2)^-} \tag{27}$$

$$T_{y=(H_1-\delta_2)^+} = T_{y=(H_1-\delta_2)^-},\ k_{eff,(H-\delta_2)^+}\left.\frac{\partial T}{\partial y}\right|_{y=(H-\delta_2)^+} = k_{eff,y=(H-\delta_2)^-}\left.\frac{\partial T}{\partial y}\right|_{y=(H-\delta_2)^-} \tag{28}$$

At the interface between the heated wall and the catalyst layers, the velocities and the concentration gradient are assumed to be zero, and the temperature is assumed to be equal to the catalyst temperature:

$$u = v = w = \frac{\partial C_i}{\partial y} = 0,\quad T = T_w \tag{29}$$

In the present study, the mass fractions of the inlet reactant gas including methanol vapor and water vapor of 0.38 and 0.62, respectively, were tested. Thus, the molar ratio of H_2O/CH_3OH was kept constant at 1.1. The inlet flow velocity of 0.266 m/s used and therefore, the corresponding Reynolds number Re was 10.98 for each test. The physical properties of the micro channels are listed in Table 2.

Table 3
Mole fractions of methanol for the various grid tests at different axial locations.

$I \times J \times K$	x (m)					
	0.005	0.010	0.015	0.020	0.025	0.030
$41 \times 18 \times 18$	0.418	0.372	0.334	0.303	0.276	0.253
$51 \times 25 \times 23$	0.419	0.372	0.335	0.304	0.277	0.254
$71 \times 35 \times 33$	0.419	0.373	0.335	0.303	0.277	0.253

3. Numerical method

A generalized form of the transport equation for mass, momentum, energy can be expressed in a conservative form as follows:

$$\frac{\partial}{\partial t}\int_V \rho\phi \, dV = \int_A \rho\phi V \, dA = \int_A \Gamma \nabla\phi \, dA + \int_\forall S_\phi \, dV \quad (30)$$

where t is the time, ϕ is a general dependent variable, S_ϕ is the source per unit volume and ρ is the density. All equations were numerically solved using the commercial fluid dynamics program, Fluent™. The SIMPLE algorithm was employed to solve the convection-diffusion equations.

The grid independence was examined in preliminary test runs. Three grid configurations were evaluated for the micro channel of the plate methanol steam micro-reformer at a wall temperature of 200 °C. The numbers of grid lines in the x, y and z directions were: $41 \times 18 \times 18$, $51 \times 25 \times 23$, and $71 \times 35 \times 33$. The influence of grid lines on the local methanol mole fraction is shown in Table 3. The deviations of methanol mole friction are 0.4% for grids $41 \times 18 \times 18$ and $51 \times 25 \times 23$, and 0.4% for grids $51 \times 25 \times 23$ and $71 \times 35 \times 33$. Grid $51 \times 25 \times 23$ was, therefore, chosen for the simulation in the present study as a tradeoff between accuracy and CPU computation time. The convergence criterions for the normalized residuals for each variable were restricted to less than 10^{-6}.

The validation of the numerical results is performed by comparing the present predictions with previous experimental results. The geometric dimensions and physical properties of the micro channel are listed in Table 2. Fig. 2 shows the comparison of the present predictions and experimental results. The solid symbols denote the experimental results of Park et al. [40] and the curve is the present prediction. The results show that the numerical results agree reasonably well with the experimental data.

4. Results and discussion

In this work, the numerical results are obtained for a micro channel of a plate methanol steam micro-reformer. Using previously stated the numerical model, the effects of aspect ratios of micro channel on methanol conversion and transport phenomena were emphasized. For aspect ratio of $\gamma = 0.5$, Fig. 3 presents the local distributions of the different species at wall temperatures of 200 and 260 °C along the center of the micro channel. Overall inspection of Fig. 3 disclosed that the CH_3OH and H_2O mole fractions decrease along the micro channel, while the H_2, CO_2 and CO mole fractions increase along the center of the micro channel. The results demonstrate that as the mole fractions of the products increase as the wall temperature increases. The results also show that the methanol conversion is about 49% for a wall temperature of 200 °C, with a gas composition of 24% CH_3OH, 28% H_2O, 36% H_2, and 12% CO_2 at the micro channel outlet. However, the CO concentration is only 244 ppm. For a wall temperature of 260 °C, the results indicates that the methanol conversion is greater than 96%, with a product gas composition of 74.05% H_2, 24.28% CO_2, and 1.67% CO at the micro channel outlet. For the PEMFC, the CO concentration must be less than 10 ppm which can be achieved using a CO oxidation reactor. The utilization of the preferential oxidizer (PrOx) reactor or water-gas-shift reaction can reduce the CO concentration in the gas from the methanol micro-reformer. Kwon et al. [6] used a reformer and PrOx reactor, and showed that the CO produced was totally removed from the gas by the PrOx device.

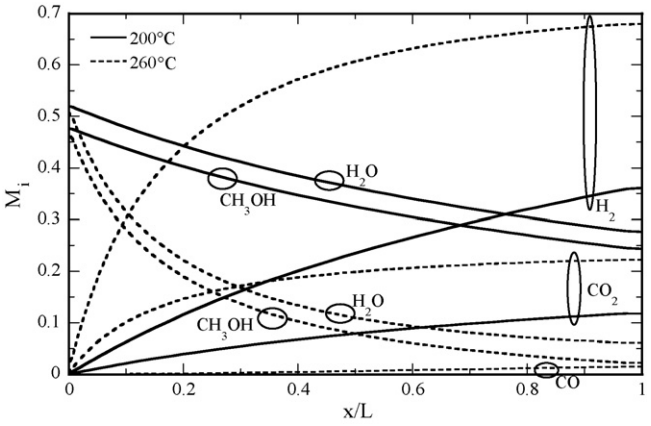

Fig. 3. Variations of the mole fractions of the various species along the micro channel center line ($\gamma = 0.5$).

Fig. 4 presents the effects of the aspect ratios of micro channel on methanol conversion and CO concentration (ppm). In this work, the catalyst thicknesses are fixed to be 30 μm. A careful examination of Fig. 4 reveals that the methanol conversion increases with an increase in wall temperature. Thus, the methanol conversion can be improved by increasing wall temperature, which in turn, increases the chemical reaction rate. It is also found form Fig. 4 that

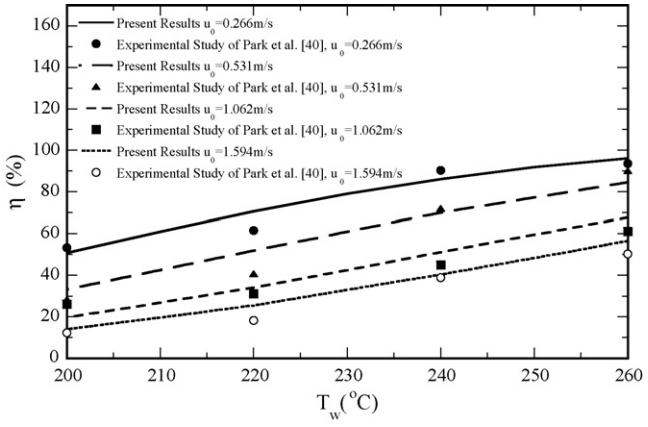

Fig. 2. Comparison of predicted methanol conversion with previous experimental data of Park et al. [40].

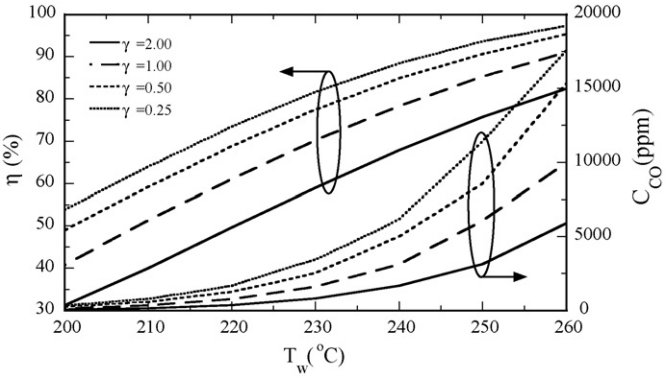

Fig. 4. Effects of aspect ratios of micro channel and wall temperature on methanol conversion and CO concentration (ppm) at outlet of micro channel.

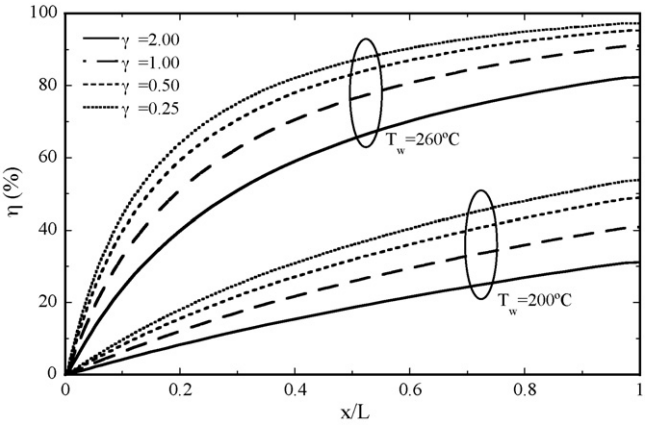

Fig. 5. Effects of aspect ratios of micro channel on the local methanol conversion along center line of micro channel at $T_w = 200\,^{\circ}C$ and $T_w = 260\,^{\circ}C$.

the methanol conversion increases with a decrease in aspect ratio due to the large chemical reaction area for a low aspect-ratio micro channel. This implies that better performance is noted for a lower aspect-ratio micro channel reformer. The CO concentration (ppm) leaving the micro channel was also studied. In Fig. 4, the results show that the CO concentration increases with increasing wall temperature. This can be made plausible by noting the fact that the reaction rate of the endothermic reverse water-gas-shift reaction increases as the wall temperature increases. Additionally, it is also found that the CO concentration (ppm) increases with decreasing aspect ratios. A height/width ratio of $\gamma = 0.25$ and a wall temperature of 260 °C yielded the better methanol conversion (greater than 98%), but the CO concentration was also higher, and was greater than 16,000 ppm. Hence, the CO concentration in the outlet gases must be reduced for further use in a PEMFC.

The effects of aspect ratios on local methanol conversion distributions along the micro channel center line at $T_w = 200\,^{\circ}C$ and $T_w = 260\,^{\circ}C$ are presented in Fig. 5. An overall inspection of Fig. 5 reveals that the aspect ratios of micro channel have a considerable impact on the local methanol conversion distributions along the center line. It is found that the predicted methanol conversion increases along the micro channel. In addition, methanol conversion efficiency increases with decreasing aspect ratios of micro channel. As for the effects of wall temperature, better methanol conversion is noted for a case with a higher wall temperature owing to a stronger chemical reaction rate.

Fig. 6 shows the effects of the aspect ratios of micro channel on the distribution of the H_2 and CO mole fractions, respectively, along the micro channel center line. It is clear in Fig. 6(a) that the H_2 mole fraction along the micro channel center line represents the methanol conversion, with a higher H_2 fraction indicating higher methanol conversion rates. Thus, the variation of the H_2 fraction is opposite to that of the CH_3OH mole fraction. It is clearly observed from Fig. 6(a) the H_2 mole fraction increases as the aspect ratio decreases and wall temperature increases. The trends of the variations in Fig. 6(b) can be interpreted in a similar way to the data in Fig. 5. This is because that a higher methanol conversion results in a higher CO production. These phenomena are more obvious at a higher wall temperature (260 °C), because the methanol micro-reformer produces more CO for a higher wall temperature.

Fig. 7(a) presents the reactant gas velocity distributions in the center of the micro channel along the direction of flow from the inlet to the outlet for wall temperatures of 200 and 260 °C for the various aspect ratios. It is clearly seen in Fig. 7(a) that the velocity slowly increases from the inlet to the outlet. The wall temperature of 260 °C generates higher gas velocity distributions than that of 200 °C. The results show that the methanol conversion of the micro-reformer is independent of the velocity distributions in the center of the micro channel due to the chemical reaction dominating methanol conversion. Then, to explore the pressure loss caused by the various aspect ratios, the local pressure losses (the difference between local and inlet pressures) along the micro channel center line for wall temperatures of 200 and 260 °C under various aspect ratios are presented in Fig. 7(b). In Fig. 7(b), it is found that the local pressure loss increases along the flow channel. A careful examination of Fig. 7(b) discloses that larger pressure loss is noticed for a case with a higher wall temperature (260 °C). Additionally, the results show that larger pressure loss is found for a smaller aspect ratio ($\gamma = 0.25$). The higher pressure losses mean that excess work has to be done in pushing the gases through. Therefore, reducing pressure losses is one of the most important issues.

Effects of the aspect ratios on the temperature distributions are shown in Fig. 8(a). It is clearly seen that the fluid temperature increases along the channel as a consequence of chemical reaction. When $x/L > 0.2$, the fluid temperature increase insignificantly along channel because there is a thermal equilibrium beyond this point. It is also shown that the temperature rises with the decrease in aspect ratios, γ. As the γ decreases, the temperature distributions become much more uniform. Therefore, a smaller aspect ratio leads to a better methanol conversion. Afterwards, to explore the change in steam reforming reaction rate caused by the various aspect ratios of the micro channels, the local steam reforming reaction rates along the interface between the catalyst layer and the flow channel are presented in Fig. 8(b). For a wall temperature of 260 °C, the steam reforming reaction rate first rises rapidly, and then declines steadily after $x/L = 0.001$. For $x/L < 0.05$, the steam reforming reaction rate increases with decreasing aspect ratios. For $x/L > 0.05$, larger

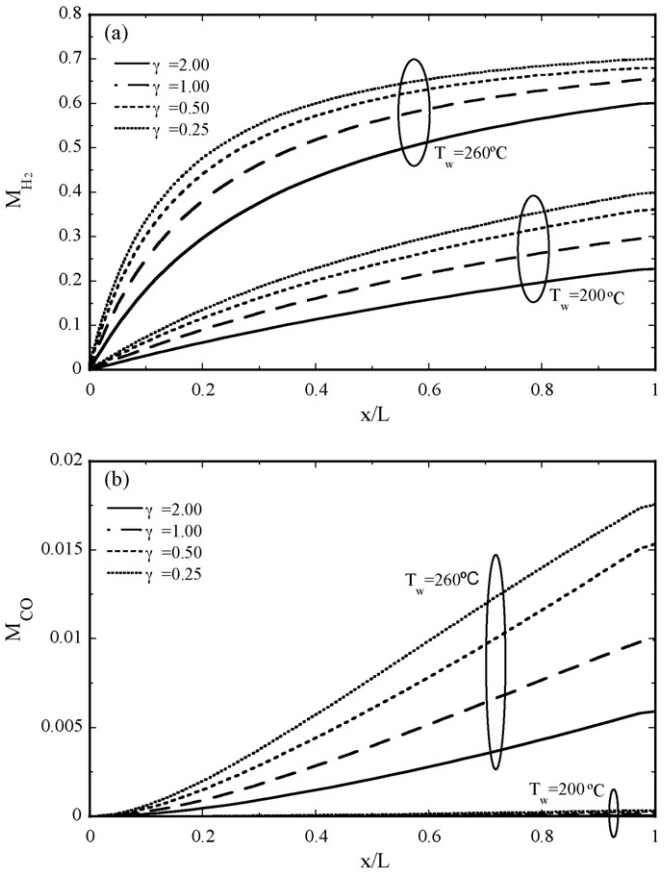

Fig. 6. Effects of aspect ratios of micro channel at $T_w = 200\,^{\circ}C$ and $T_w = 260\,^{\circ}C$ on (a) local H_2 mole fraction and (b) local CO mole fraction along center line of micro channel.

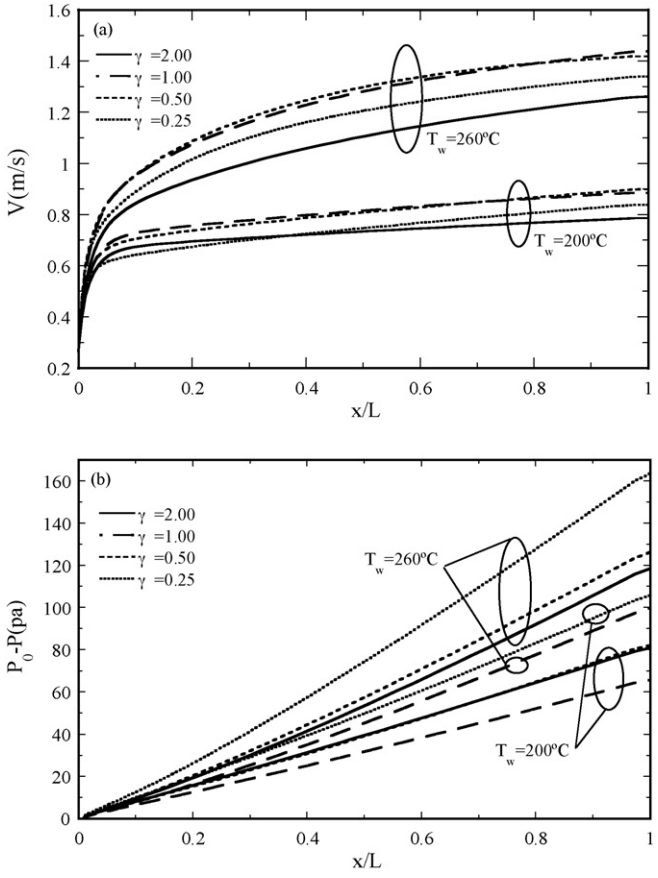

Fig. 7. Effects of aspect ratios of micro channel at T_w = 200 °C and T_w = 260 °C on (a) local velocity and (b) local pressure along center line of micro channel.

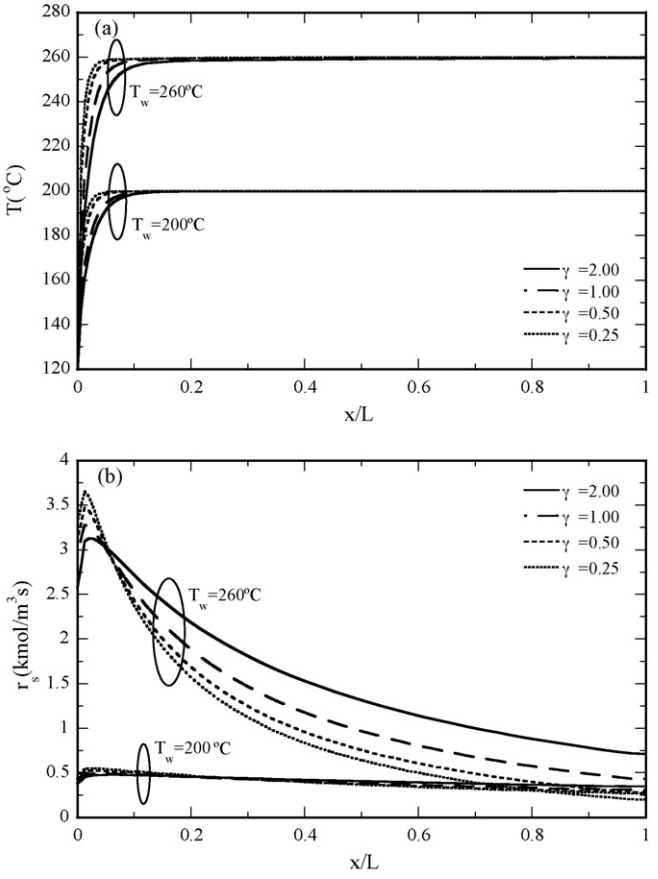

Fig. 8. Effects of aspect ratios of micro channel at T_w = 200 °C and T_w = 260 °C on (a) local temperature along center line of micro channel and (b) local reaction rates of methanol steam reforming along interface between flow channel and catalyst layer.

aspect ratios can improve the steam reforming reaction rate, as a result of the methanol being consumed in the forward region of micro channel inlet. For a lower wall temperature of 200 °C, the change in steam reforming reaction rate follows a similar trend to that of the wall temperature 260 °C. In addition, it is found that a higher steam reforming reaction rate is found for a case with a higher wall temperature due to a stronger steam reforming reaction.

Fig. 9 demonstrates the effects of the Reynolds number on the methanol conversion and the H_2 production rate of the micro channel in the plate methanol steam micro-reformer for wall temperatures of 260 °C. An overall inspection of Fig. 9 discloses that the methanol conversion increases with decreasing Reynolds number Re. This can be made plausible by noting the fact that the fuel can spend more time in the micro channel for a lower Reynolds number Re. As for the H_2 production rate, the results show that the H_2 production rate increases as the Re increases. Additionally, the effects of the aspect ratios on the methanol conversion and H_2 production rate are shown in Fig. 9. It is clear that the methanol conversion increases with a decrease in aspect ratio. When $\gamma = 0.25$ with a Re of 22, the methanol conversion was greater than 86%, and the H_2 production rate was 231 cm^3/min. The plate methanol steam micro-reformer produced hydrogen to supply fuel cell, Park et al. [40] presented that the H_2 production rate was only 186 cm^3/min, which could supply a 15 W fuel cell.

Effects of geometric size on the transport phenomena and performance of micro-reformer are important. To this end, the effects of micro channel size on temperature distributions are shown in Fig. 10. In Fig. 10, two micro channel sizes were tested: micro channel (I) 33 mm(L) × 1.5 mm(W) × 0.75 mm(H) and micro channel (II) 33 mm(L) × 0.429 mm(W) × 0.214 mm(H), respectively. The aspect ratios were all fixed to be 0.5, with the catalyst thickness being 30 μm. Different micro channel sizes have different hydraulic diameters. Micro channel (I) has a greater hydraulic diameters than micro channel (II). It is found from Fig. 10 that the temperature distribution increases along the micro channel as a consequence of the chemical reaction. For a smaller micro channel size, the temperature distribution is much more uniform due to the shorter thermal entrance length. This kind of uniform temperature distribution improves the chemical reaction rate. As a result, the smaller micro channel leads to better methanol conversion. Comparing the local temperature distributions for wall temperatures of 200 and 260 °C,

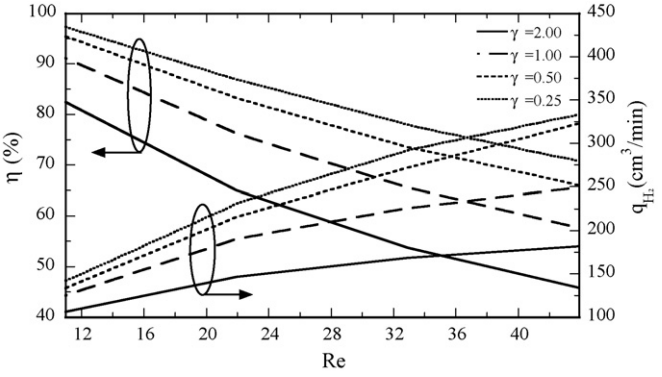

Fig. 9. Effects of aspect ratios of micro channel and Reynolds number on methanol conversion and H_2 production rate at T_w = 260 °C.

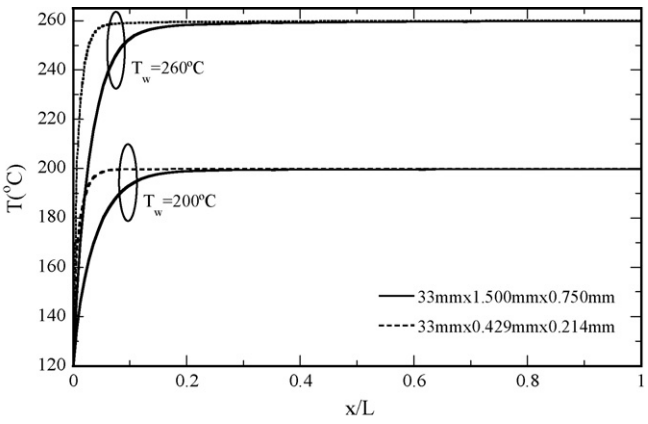

Fig. 10. Effects of geometric size of micro channel on local temperature along center line of micro channel at T_w = 200 °C and T_w = 260 °C.

it can be shown that the local temperature distribution increases with increasing wall temperature.

The effects of the Reynolds number Re on the methanol mole fraction distributions of two micro channel sizes (I) 33 mm(L) × 1.5 mm(W) × 0.75 mm(H) and (II)33 mm(L) × 0.429(W)mm × 0.214 mm(H) for wall temperatures of 200 and 260 °C are examined in Fig. 11. The results show that a larger CH_3OH mole fraction is noted for a case with a higher Reynolds number Re. Additionally, it is clearly observed that for fixed Re, micro channel (I) shows similar methanol distributions to those of micro channel (II). Therefore, micro channels (I) and (II) have similar methanol conversion, but micro channel (I) requires more catalyst loading and a slower velocity than micro channel (II). This is because that micro channel (II) has a more uniform temperature distribution which increases the chemical reaction rate. Comparison of Fig. 11(a and b) shows that the CH_3OH consumption increases with increasing wall temperature, which in turn, increases the reaction rate.

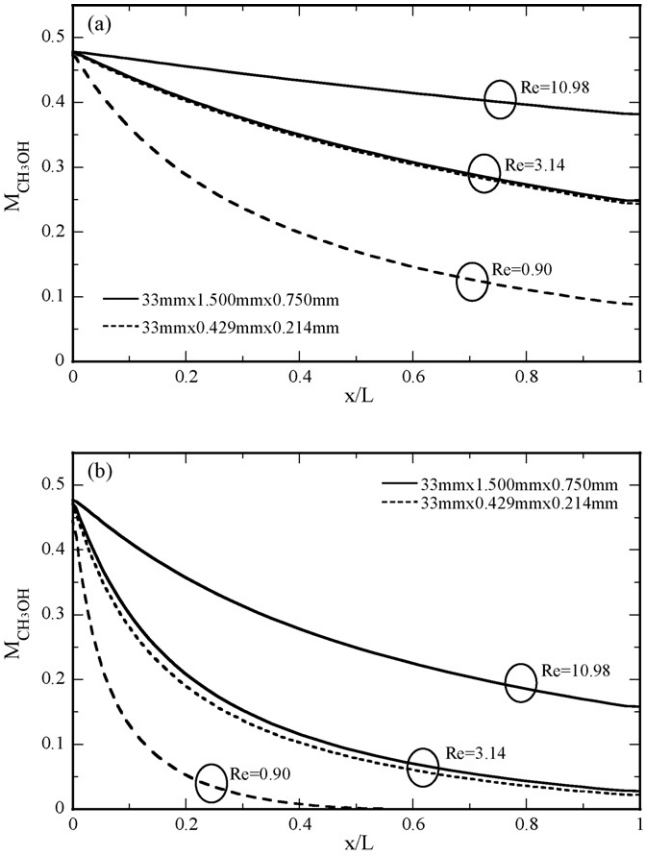

Fig. 11. Effects of geometric size of micro channel and Reynolds number on local CH_3OH mole fraction along center line of micro channel at (a) T_w = 200 °C and (b) T_w = 260 °C.

5. Conclusions

A three-dimensional micro channel model was developed to investigate the geometric sizes (aspect ratios and micro channel size) and thermo-fluid parameters (Reynolds number and wall temperature) on methanol conversion and local transport phenomena in the micro channel of a plate steam methanol micro-reformer. The conclusions are as follows:

1. A reduction in the aspect ratio (γ) improves H_2 production rate and methanol conversion.
2. A decrease in the aspect ratio can increase methanol consumption and the hydrogen mole fraction along the micro channels. A reduction in the aspect ratio also yields a much more uniform temperature distribution, while also increasing the steam reforming reaction rate and methanol conversion.
3. The better methanol conversion and the H_2 production rate are noted for the smaller aspect ratio.
4. Smaller micro channels have much more uniform temperature distributions, which in turn, result in a decrease in the thermal entrance lengths. Therefore, fuel utilization efficiency is improved for a small micro channel.
5. For the same hydraulic diameter, a reduced Re increases the reactant gas residence time, which in turn increases the reaction time and significantly increases methanol conversion.

References

[1] A. Kundu, J.H. Jang, J.H. Gil, C.R. Jung, H.R. Lee, S.H. Kim, B. Ku, Y.S. Oh, J. Power Sources 170 (2007) 67–78.
[2] J.D. Holladay, Y. Wang, E. Jones, Chem. Rev. 104 (2004) 4767–4790.
[3] G. Kolb, V. Hessel, V. Cominos, C. Hofmann, H. Lowe, G. Nikolaidis, R. Zapf, A. Ziogas, E.R. Delsman, M.H.J.M. De Croon, J.C. Schouten, O. De La Iglesia, R. Mallada, J. Santamaria, Catal. Today 20 (2007) 2–20.
[4] J.W. Ha, J.H. Jang, J.H. Gil, S.H. Kim, Int. J. Hydrogen Energy 33 (2008) 2059–2063.
[5] M.S. Lim, M.R. Kim, J. Noh, S.I. Woo, J. Power Sources 140 (2005) 66–71.
[6] O.J. Kwon, S.M. Hwang, J.H. Chae, M.S. Kang, J.J. Kim, J. Power Sources 165 (2006) 342–346.
[7] O.J. Kwon, D.H. Yoon, J.J. Kim, Chem. Eng. J. 140 (2008) 466–472.
[8] G.G. Park, S.D. Yim, Y.G. Yoon, C.S. Kim, D.J. Seo, K. Eguchi, Catal. Today 110 (2005) 108–113.
[9] K. Yoshida, S. Tanaka, H. Hiraki, M. Esashi, J. Micromech. Microeng. 16 (2006) 191–197.
[10] B.A. Peppley, J.C. Amphlett, L.M. Kearns, F.M. Ronald, Appl. Catal. A 179 (1999) 21–29.
[11] A. Mastalir, B. Frank, A. Szizybalski, H. Soerijanto, A. Deshpande, M. Niederberger, R. Schomäcker, R. Schlögl, T. Ressler, J. Catal. 230 (2005) 464–475.
[12] J.K. Lee, J.B. Ko, D.H. Kim, Appl. Catal. A 278 (2004) 25–35.
[13] Y. Kawamura, N. Ogura, T. Yamamoto, A. Igarashi, Chem. Eng. Sci. 61 (2006) 1092–1101.
[14] T. Kim, S. Kwon, J. Micromech. Microeng. 16 (2006) 1760–1768.
[15] A. Varesano, I. Guaglio, G. Saracco, P.L. Maffettone, Ind. Eng. Chem. Res. 44 (2005) 759–768.
[16] A.V. Pattekar, M.V. Kothare, J. Power Sources 147 (2005) 116–127.
[17] A.T. Stamps, E.P. Gatzke, J. Power Sources 161 (2006) 356–370.
[18] J.R. Lattner, M.P. Harold, Catal. Today 120 (2007) 78–89.
[19] J.C. Amphlett, K.A.M. Creber, J.M. Davis, R.F. Mann, B.A. Peppley, D.M. Stokes, Int. J. Hydrogen Energy 19 (1994) 131–137.
[20] A. Peppley, J.C. Amphlett, L.M. Kearns, R.F. Mann, Appl. Catal. A179 (1999) 31–49.
[21] T.L. Reitz, S. Ahmed, M. Krumpelt, R. Kumar, H.H. Kung, J. Mol. Catal. A: Chem. 162 (2000) 275–285.
[22] J.S. Suh, M.T. Lee, R. Greif, C.P. Grigoropoulos, J. Power Sources 173 (2007) 458–466.
[23] A. Karim, J. Bravo, A. Datye, Appl. Catal. A282 (2005) 101–109.
[24] A. Karim, J. Bravo, D. Gorm, T. Conant, A. Datye, Catal. Today 110 (2005) 86–91.
[25] C. Cao, Y. Wang, J.D. Holladay, E.O. Jones, D.R. Palo, AlChE J. 51 (2005) 982–988.
[26] L. Pan, S. Wang, Chem. Eng. J. 108 (2005) 51–58.
[27] A.V. Pattekar, M.V. Kothare, J. Microelectromech. Syst. 13 (2004) 7–18.

[28] H.G. Park, J.A. Malen, W.T. Piggott III, J.D. Morse, R. Greif, C.P. Grigoropoulos, J. Microelectromech. Syst. 15 (2006) 976–985.
[29] C. Cao, G. Xia, J. Holladay, E. Jones, Y. Wang, Appl. Catal. A 262 (2004) 19–29.
[30] M. Zanfir, A. Gavriilidis, Chem. Eng. Sci. 58 (2003) 3947–3960.
[31] J. Yuan, F. Ren, B. Sunden, Int. J. Heat Mass Transfer 50 (2007) 687–701.
[32] M.J. Stutz, N. Hotz, D. Poulikakos, Chem. Eng. Sci. 61 (2006) 4027–4040.
[33] H.C. Yoon, J. Otero, P.A. Erickson, Appl. Catal. B75 (2007) 269–276.
[34] O.L. Ding, S.H. Chan, Int. J. Hydrogen Energy 33 (2008) 633–643.
[35] A.P. Kagyrmanova, I.A. Zolotarskii, E.I. Smirnov, N.V. Vernikovskaya, Chem. Eng. J. 134 (2007) 228–234.
[36] D.D. Davieau, P.A. Erickson, Int. J. Hydrogen Energy 32 (2007) 1192–1200.
[37] A. Kundu, J.H. Jang, H.R. Lee, S.H. Kim, J.H. Gil, C.R. Jung, Y.S. Oh, J. Power Sources 162 (2006) 572–578.
[38] S. Ergun, Chem. Eng. Prog. 48 (1952) 89–94.
[39] H. Purnama, T. Ressler, R.E. Jentoft, H. Soerijanto, R. Schlogl, R. Schomacker, Appl. Catal. A 259 (2004) 89–94.
[40] G.G. Park, D.J. Seo, S.H. Park, Y.G. Yoon, C.S. Kim, W.L. Yoon, Chem. Eng. J. 101 (2004) 87–92.